Extracting transverse electron mean free paths in graphene at low energy

Neu, P.S.; Geelen, D.; Tromp, R.M.; Molen, S.J. van der

Citation
Neu, P. S., Geelen, D., Tromp, R. M., & Molen, S. J. van der. (2023). Extracting transverse electron mean free paths in graphene at low energy. *Ultramicroscopy*, *253*. doi:10.1016/j.ultramic.2023.113800

Version:	Publisher's Version
License:	Creative Commons CC BY 4.0 license
Downloaded from:	https://hdl.handle.net/1887/3718517

Note: To cite this publication please use the final published version (if applicable).

Ultramicroscopy 253 (2023) 113800

Contents lists available at ScienceDirect

Ultramicroscopy

journal homepage: www.elsevier.com/locate/ultramic

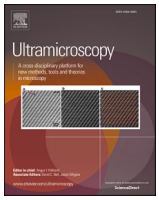

Extracting transverse electron mean free paths in graphene at low energy

Peter S. Neu [a], Daniël Geelen [a], Rudolf M. Tromp [b,a], Sense Jan van der Molen [a,*]

[a] Leiden Institute of Physics, Universiteit Leiden, Niels Bohrweg 2, Leiden, the Netherlands
[b] IBM Research, T.J. Watson Research Center, 1101 Kitchawan Road, Yorktown Heights, NY 10598, USA

ARTICLE INFO

Keywords:
LEEM
eV-TEM
Graphene
Interference model
Mean free path
Plasmon

ABSTRACT

The LEEM-IV spectra of few-layer graphene show characteristic minima at specific energies, which depend on the number of graphene layers. For the same samples, low-energy TEM (eV-TEM) spectra exhibit transmission maxima at energies corresponding to those of the reflection minima in LEEM. Both features can be understood from interferences of the electron wave function in a purely elastic model. Inelastic scattering processes in turn lead to a finite, energy-dependent inelastic Mean Free Path (MFP) and a lower finesse of the interference features. Here we develop a model that introduces both an elastic and inelastic scattering parameter on the wave-function level, thus reconciling the models considered previously. Fitting to published data, we extract the elastic and inelastic MFP self-consistently and compare these to recent reports.

1. Introduction

The (inelastic) electron Mean Free Path (MFP) is a material-specific quantity describing the mean distance of free travel by an electron until it scatters (inelastically). In the case of a bulk material and an electron incident from vacuum, one can to first approximation expect an exponential decay of the electron flux with increasing thickness. The MFP with respect to energy was generally found to follow a U-shape curve in a broad selection of materials [1]. This so-called universal curve [2] runs over a large energy range, up to 10^6 eV, and has a single minimum around 30–50 eV. However, recent studies of 2D materials, foremost graphene, have shown additional features to the energy-dependent MFP curve, especially at low energies where the electron wavelength is on the order of the lattice spacings [3–6]. An increasing interest in properties and applications of (heterostructures of) 2D materials, as well as in inelastic interaction of low-energy electrons with nanolayers, calls for a consistent description of scattering effects in these quantum systems.

Recently, experimental reflectivity and transmissivity data on 1-4 layers of graphene have been published by Geelen et al. [4]. In that study, Low Energy Electron Microscopy (LEEM) was used to obtain reflection spectra $R(E)$, while electronVolt-Transmission Electron Microscopy (eV-TEM) was introduced to obtain transmission curves $T(E)$ (see Fig. 1a). Here, E denotes the electron energy with respect to the vacuum energy, defined as $E_{vac} = 0$. For multilayers (two or more atomic layers) of graphene, both $R(E)$ and $T(E)$ curves revealed interference effects, thus calling for a wave-based scattering model. From the difference between unity and the sum of reflection and transmission, inelastic scattering effects were quantified. Thus, the authors determined the inelastic MFP (IMFP) as a function of energy, directly from reflectivity and transmissivity spectra. More recently, Yang et al. [7] argued against the methodology chosen by Geelen et al. to determine the IMFP and re-analyzed the experimental data using an alternative method. Specifically, they applied a correction factor to take into account the zig-zag path the electron travels between multiple reflections. Within their analysis, they conclude that a $\pi + \sigma$ plasmon in multilayer graphene is discernible in Geelen et al.'s data. This $\pi + \sigma$ plasmon cannot be excited in the monolayer [8].

The jellium-like model used by Yang et al. has clear advantages with respect to the method Geelen et al. used. Specifically, the statistical average of the path travelled by an electron until it randomly scatters inelastically was developed in their model. Fundamental to the jellium-like model, however, is that it cannot account for the interference effects [9] that are characteristic of the multilayer graphene system.

Here we introduce an improved method to reconcile these two previous models. Our approach is to keep the notion of discrete graphene layers intact while incorporating an inelastic loss factor that relates to the zig-zag path travelled by the electron between graphene layers. By fitting this model to the data published in reference [4], we extract the inelastic MFP and a reflection coefficient of the electron wave function in a one-step process. We also discuss whether the $\pi + \sigma$ plasmon can indeed be extracted from the data available.

* Corresponding author.
E-mail address: molen@physics.leidenuniv.nl (S.J. van der Molen).

https://doi.org/10.1016/j.ultramic.2023.113800
Received 23 January 2023; Received in revised form 2 June 2023; Accepted 19 June 2023
Available online 20 June 2023
0304-3991/© 2023 The Author(s). Published by Elsevier B.V. This is an open access article under the CC BY license (http://creativecommons.org/licenses/by/4.0/).

2. Interference model with losses

To obtain some intuition for the problem, we will first consider single-layer graphene. Along the propagation direction of the electron, perpendicular to the atomic plane, the scattering problem then resembles a well-known quantum-mechanics exercise: calculating the (unbound) states of a one-dimensional potential well [10]. The extension of this calculation to multiple wells equivalent to multiple graphene layers can then be done by a transfer matrix approach [11]. Further simplifying this model, one can compare each graphene layer to a partially transparent mirror in an optical Fabry-Pérot experiment [12], leading to a series of resonances as a function of wavelength and hence energy. Fig. 1b illustrates the partial reflection (transmission) of the electron wave incident upon a graphene layer (orange plane) with reflection and transmission coefficients r and t. As there is no cutoff to the number of partial reflections, the reflected/transmitted flux is the absolute square of an infinite sum of interfering waves. Conservation of flux at the layer requires , with $r, t < 1$. Note that in the experiment by Geelen et al. (see sketch Fig. 1a) the electron beams incident on the graphene from either side were aligned perpendicularly to the sample and a contrast aperture was inserted to block electrons that lost energy or were scattered off-axis.

Generally, interference effects will depend on electron energy via the de Broglie electron wavelength. At wavelengths for which interferences are constructive in the forward direction, transmission maxima will be found. Thus, the so-called interference 'toy-model' introduced by Geelen et al. provides a basic explanation for the presence of transmission peaks and (accompanying) reflection minima in the experimental curves, which occur around 3 eV and 18 eV (see Fig. 3).

For our discussion, we first need to consider this toy-model in more detail. The phase propagation over a distance equal to the layer spacing a is given by:

$$\varphi = a \cdot \sqrt{\frac{2m_e}{\hbar^2}(E + \Phi)}, \tag{1}$$

where E is the incident electron energy (with respect to the vacuum level) and $\Phi = 4.6$ eV (which is close to the work function), the free electron mass and $\hbar$the reduced Planck constant [13]. The quantum mechanical reflectivity and transmissivity coefficients of n layers (see supplemental material in [4]) yield the following recursive formulas:

$$t_n = \left[\frac{t \cdot t_{n-1} e^{i\varphi}}{1 + r \cdot r_{n-1} e^{2i\varphi}}\right] \tag{2a}$$

$$r_n = \left[r + \frac{t^2 \cdot r_{n-1} e^{2i\varphi}}{1 + r \cdot r_{n-1} e^{2i\varphi}}\right] \tag{2b}$$

with r and the wave reflection and transmission coefficients for a single layer within the structure. Obviously, for the case of single layer graphene, $r_1 = r$ and $t_1 = t$, respectively. The measured electron intensities for n layers of graphene are finally obtained by taking the absolute square of the wave function, $T_n = |t_n|^2$ and $R_n = |r_n|^2$.

However, the formulas used by Geelen et al. to extract the total and inelastic MFP (Eq. (1) and (2) in [4]) were not linked to this toy-model. Rather, the authors chose a more macroscopic picture. As Yang et al. criticize, Eq. (1) and (2) in [4] combined imply that both the transmitted and reflected electrons travel a distance equal to the sample thickness d through the material, which is a reasonable assumption for the transmitted electrons but not for the reflected electrons. Furthermore, we point out that Eq. (2) in [4], reading $T + R = \exp(-d/\lambda_{\text{inel}})$ cannot hold for bulk, as it implies that no electrons are transmitted nor reflected, while LEEM experiments show that there is reflection from bulk samples (in fact several nanometers of thickness can be considered as bulk: after that the reflectivity barely changes, possibly being as large as 50%, e.g., in graphene on silicon carbide [13]).

Yang et al. also emphasize that the path travelled by an electron may be much larger than the material thickness, as the partial reflection and transmission leads to zig-zag paths (see Fig. 1c for an example path). They propose a correction factor (Fig. 1c in [7]) that depends on the experimentally obtained elastic MFP, thus the number of internal reflections. This correction factor is developed in a V-trajectory, where the block of graphene is treated as 'jellium'-like material, so scattering is equally possible anywhere inside the material. However, in such a jellium material no interference effects can occur, which is a severe limitation to their model.

The aim of this study is to reconcile both approaches. For this, we start with Geelen et al.'s toy model, and extend it to account for inelastic losses. This has the advantage that interferences are possible, while inelastic processes – which, e.g., lead to a loss of finesse and thus a broadening of the peaks in the interference system - are considered more accurately. We introduce an inelastic loss factor β for every reflection or transmission event. While the losses upon reflection and transmission may in principle be different, fitting β and r already allows for this freedom (without introducing redundant parameters). By using only one factor β, $(1-\beta)^2$ can be interpreted as the loss in electron flux per unit cell length a travelled (see Fig. 2). Still the elastic backscattering events only take place at the discrete graphene layers, keeping the interference condition intact. Effectively this means replacing r and t by βr and βt [r_{n-1} and t_{n-1} remain unchanged, as the factor β is already included

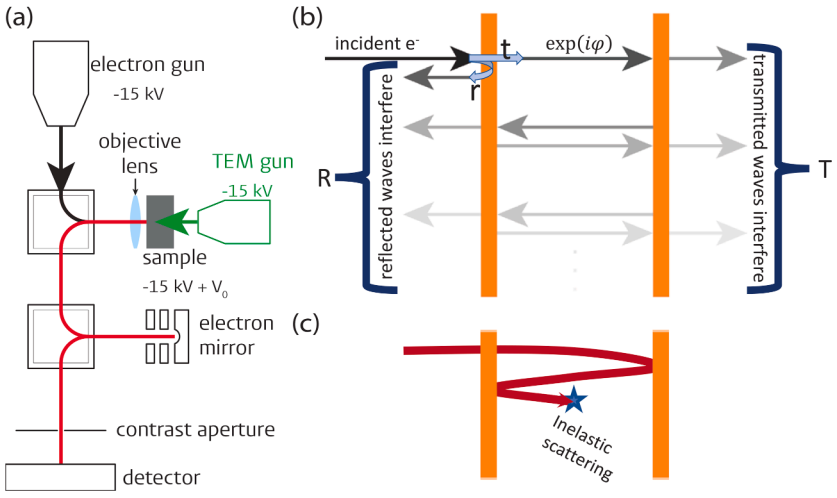

Fig. 1. (a) sketches the LEEM setup, with the path of the incident electrons in LEEM mode (black) and in eV-TEM mode (green). After reflection/transmission from the sample the electrons follow the red path to the detector. (b) Illustration of the electron paths through two layers of graphene upon multiple partial reflections and transmissions. Between the layers, the electron wave gains a phase φ. (c) One classical electron trajectory (red path). After travelling some distance (on average: the inelastic Mean Free Path (IMFP)), an inelastic scattering process happens. Experimentally, this means that the electron is not detected in reflection nor transmission. Analysis of the IMFP is required to take into account such 'zig-zag paths' [6], which may be significantly longer than the thickness of the material.

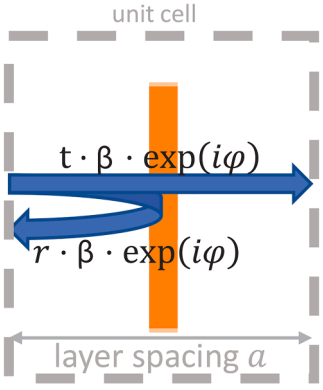

Fig. 2. Illustration of the improved interference model. Each graphene layer (orange) partially transmits (reflects) the electron wave function with fraction t (fraction r). Over a layer distance a the phase propagates by φ and the amplitude is damped by the loss factor β. For multilayer graphene, this 'unit cell' is repeated.

inside them in the previous iteration] in Eqs. (2a) and (2b), so the modified recursion formulas including β are:

$$t_n = \left[\frac{\beta t \cdot t_{n-1} e^{i\varphi}}{1 + \beta r \cdot r_{n-1} e^{2i\varphi}}\right] \tag{3a}$$

$$r_n = \left[\beta r + \frac{\beta^2 t^2 \, r_{n-1} e^{2i\varphi}}{1 + \beta r \cdot r_{n-1} e^{2i\varphi}}\right] \tag{3b}$$

with $r_1 = \beta r$ and $t_1 = \beta t$. We will use the recursive formulas Eq. (3a/b) to extract the wave reflection coefficient r and the loss factor β for each energy and layer count n.

3. Results

The reflection and transmission spectra $R_n(E)$ and $T_n(E)$ for each energy were calculated from Eq. (3a/b) (absolute squared) and fitted to the experimental data from Geelen et al. (see Fig. 3a/b) using a least square fitting routine with r and β as the only fitting parameters. The resulting fit has zero degrees of freedom, as there are only two unknowns, $r(E)$ and $\beta(E)$, at each energy and the two electron intensities $R_n(E)$ and $T_n(E)$ have been measured. Thus, the fit actually is the result of numerically solving these two equations ($R(E)$ and $T(E)$) with two unknowns ($r(E)$ and $\beta(E)$). The fitting code, that invokes the *scipy.optimize.leastsq* routine in the SciPy [14] package, is provided as a python notebook file in the supplementary material. The initial guess of $r(E)$ and $\beta(E)$ was estimated from the analytical solution of the one-layer case. After a maximum of 100 iterations, the fit has converged for all datasets except for the 4-layer dataset above 23 eV. These non-converged fits have been disregarded, as the pair of R and T values at that energy falls outside the solution space of our model, even with zero degrees of freedom. We attribute this to the low intensity of the (transmitted) electrons, where the noise is comparable to the detector dark count and note that the same applies for the model of Yang et al. at the same datapoints (as seen in the absent data points for the four layer inelastic and elastic MFP in Figs. 2a and 3 of [7], respectively).

The best fit in R and T is shown in Fig. 3 c/d, and the fit parameters obtained are shown in Fig. 3e/f. The extracted loss factor β (Fig. 3e) decreases from nearly 1, i.e., no inelastic loss, at 0 eV to about 0.25 (i.e. 75% loss) for all layer counts. However, the multilayer β spectra follow a distinctly different line from the rather flat monolayer curve, deviating to higher values (less loss) between 2–8 eV and 12–25 eV. The wave reflectivity amplitude r (Fig. 3f) is rather constant for all layer counts up to 13 eV, ranging from $r = 0.3$ to $r = 0.55$. The interference peaks around 3 eV do not show up in the extracted r. At energies above 13 eV, the monolayer curve diverges from the multilayer curves, with the monolayer curve monotonically increasing to 1, while the multilayer $r(E)$ curves sharply drop to 0.15 around 18 eV and then increase to 0.4 at 25 eV.

For comparison to previously derived MFPs, we can now calculate the inelastic MFP directly from β, and the elastic MFP from t. By the relation between wave function and probability density, the inelastic loss factor in electron flux is $|\beta|^2 = \beta^2$. As the inelastic loss takes place once within each interlayer spacing a, the inelastic MFP λ_{inel} is obtained from

$$\exp(-a/\lambda_{\text{inel}}) = \beta^2 \Leftrightarrow \lambda_{\text{inel}}/a = \frac{-1}{2 \cdot \ln \beta} \tag{4}$$

With the same reasoning for the transmissivity t, the elastic MFP λ_{el} is obtained from

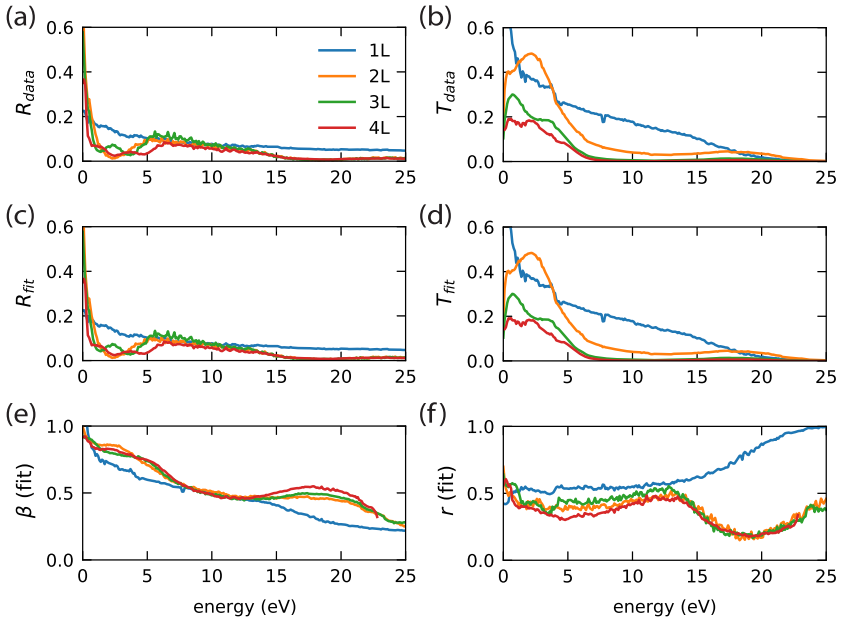

Fig. 3. Reflectivity (a) and transmissivity (b) data reproduced from Geelen et al. [4]. Best fit of the reflection/transmission equations (panel c, d) to the reflection/transmission data set (panel a,b). The energy-dependent loss parameter β (panel e) and wave reflectivity r (panel f) were obtained by fitting the improved model (Eq. 3) to the transmission and reflection data. This fit, with zero degrees of freedom, was performed for each layer count independently. The fit reproduces the dataset very well, except for the 4-layer data above 23 eV (omitted from plots above 23 eV in panels e and f).

$$\exp(-a/\lambda_{el}) = t^2 = 1 - r^2 \Leftrightarrow \lambda_{el}/a = \frac{-1}{2\cdot\ln t}. \quad (5)$$

The total MFP then follows from

$$a/\lambda_{tot} = a/\lambda_{inel} + a/\lambda_{el} = -2\ln\beta - 2\ln t = -2\ln(\beta t) \quad (6)$$

which is consistent with interpreting $(\beta t)^2$ as the total flux transmitted through a single layer after elastic and inelastic scattering.

The calculation of the inelastic MFP was the focus of the work of Yang et al. [7]. The inverse inelastic MFP they obtained is shown in Fig. 4a, alongside the inverse inelastic MFP obtained in the present study (Fig. 4b, from the fitted β). For the multilayers of graphene, the curves obtained in both studies are basically identical. Also, the monolayer curves of both studies resemble each other up to 15 eV. However, they differ at higher energies. While the curve calculated by Yang et al. increases rapidly, the curve obtained here re-joins the multilayer curves again at ~25 eV. Thus, the increase of the inverse inelastic MFP in multilayers from 5 to 15 eV (with respect to $E_{vac} = 0$) looks less unique in our analysis than in the one by Yang et al., where it was attributed to the excitation of the $\pi + \sigma$ plasmon. In our analysis the maximum in inverse inelastic MFP is rather caused by the surrounding local minima. The position of these local minima coincides with the maxima in transmissivity in the multilayer data (Fig. 3b). The fact that these local minima show up in the multilayer and not in the monolayer data suggests that they are actually caused by interference of the wave function. While the construction of the model should account for all interference effects, broadening of spectral features in the experiment can move interference effects into the fitting parameters. Also, a scattering effect that is non-linear with the electron flux 'trapped' in the cavity would show up in the fitting parameter β. That is, in the semi-classical picture of Fig. 2, we assume a constant damping factor β for each subsequent reflection between two neighboring layers (Fig. 1). The peaks in β in the 2–7 and 15–22 eV energy windows (where the transmission resonances occur) indicate that inelastic excitations in subsequent reflections/transmissions may in fact be suppressed.

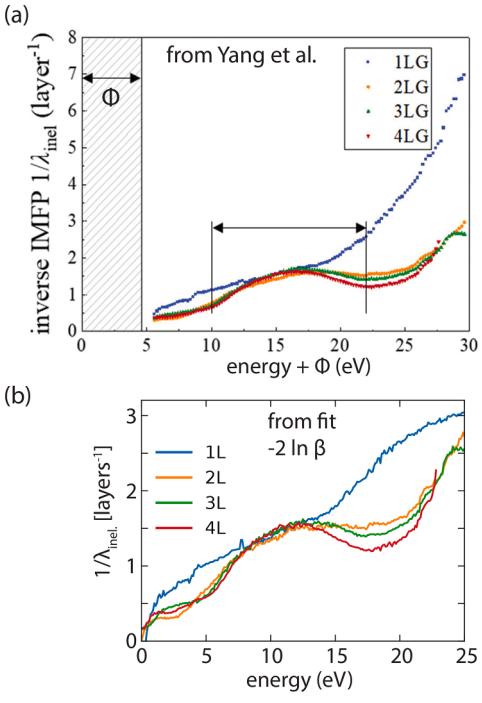

Fig. 4. Comparison of the inverse IMFP as extracted by (a): Yang et al. (plot reproduced from [7], with the permission of AIP Publishing) and (b): present analysis. The energy scales are aligned as Yang et al. use the Fermi level as the reference, which is shifted by the work function from the vacuum level. Allowing for different loss factors β upon reflection and transmission leads to physically meaningful solutions only within a range of 20% and does not alter the features of the IMFP curve.

While the $\pi + \sigma$ plasmon in multilayer graphene has been calculated [15] and observed [16,17] around 15 eV, it is unclear how it would affect the inelastic MFP-dependence on the energy of the incident electrons. Whereas EELS spectra, e.g. [18,19], show electron intensity as a function of the *energy loss of the scattered electron*, e.g., the loss to a plasmon, the inelastic MFP is a function of *the energy of the incident electron*. In other words, the electrons that are lost from the perpendicularly reflected and transmitted beam at a given energy, make up the total EELS spectrum (integrated over all energy losses) plus electrons scattered elastically over a sufficiently large angle to no longer pass through the contrast aperture. Thus, one might expect to observe a plasmon excitation as a step in the inverse inelastic MFP, at the lowest incident energy that is sufficient to excite that plasmon. At higher incident energies the plasmon can still be excited; actually, the scattering cross section generally grows with energy. To see a local maximum in inverse inelastic MFP, one must argue that the excitation of the plasmon is resonantly enhanced. We are not aware of calculations/studies that support this (at the lowest possible energy for excitation of this plasmon). The fact that the IMFP curve for the monolayer matches the curves for the multilayer IMFPs at the energies where the $\pi + \sigma$ plasmon should decrease the multilayer IMFP exactly in both Yang et al.'s and in our new analysis further refutes the interpretation as a plasmon loss.

We conclude that the features in the inelastic MFP curve of the multilayers cannot with any certainty be attributed to the $\pi + \sigma$ plasmon, and must more likely be attributed to non-linear effects due to constructive/destructive interference of the electron waves alternating with incident electron energy. However, the general trend and magnitude of the inelastic MFP curve is robust in the different analyses, running from close to no loss at 0 eV to $1/\lambda_{tot} \approx 3$ [layers^{-1}] at 25 eV.

The total MFP includes elastic and inelastic scattering. The graph obtained by Geelen et al. (calculated from $T = \exp(-d/\lambda_{tot})$, Eq. (1) in [4]) is shown in Fig. 5a, alongside our new analysis (from the fitted t and β following Eq. 6) in Fig. 5b. Both analysis methods yield similar values for λ_{tot} in the order of a few layer thicknesses. The interference peaks around 3 eV are more visible in the analysis of Geelen et al., but they still show up in our analysis (where they are mostly absorbed in the improved model). As a result, the total MFP in our analysis is rather flat up to 4 eV for the multilayers, ranging from 1.5 to 2 layer thicknesses. At energies above 10 eV and in the monolayer case the two analysis methods yield the same numbers.

The elastic MFP is the most striking result in the analysis of Geelen et al. [4] (reproduced in Fig. 6a), sharply rising at the transmission resonances. Note that in Geelen et al.'s definition the elastic MFP is not a material property of an individual layer, but rather a macroscopic way of describing the interferences in n layers of graphene. To check consistency with Geelen et al.'s model, we calculate the elastic MFP according to $\lambda_{el}^{-1} = \lambda_{tot}^{-1} - \lambda_{inel}^{-1}$ from the total MFP of Geelen et al. (which closely resembles the total MFP obtained in the present study, see Fig. 5) and the inelastic MFP obtained from fitting β (which resembles its counterpart in Yang et al.'s study, at least for the multilayer). The result is shown in Fig. 6b. In this analysis the maxima of elastic MFP around 3 eV and 18 eV are much broader than in Geelen et al.'s analysis and the curves for different layer counts fall closer together, indicating that they describe a material property less dependent on layer count.

Finally, the elastic MFP in Fig. 6c directly follows from the fit parameter t, according to Eq. (5). In the elastic MFP obtained from t, the multilayer $\lambda_{el}(E)$ shows a maximum of 30–40 layers around 18 eV and a rather smaller increase around 5 eV. The fact that no sharp maxima appear around the first transmission resonance around 3 eV indicates that the interferences are fully accounted for in the improved model.

While Geelen et al.'s elastic MFP (Fig. 6a) peaks highest at the first

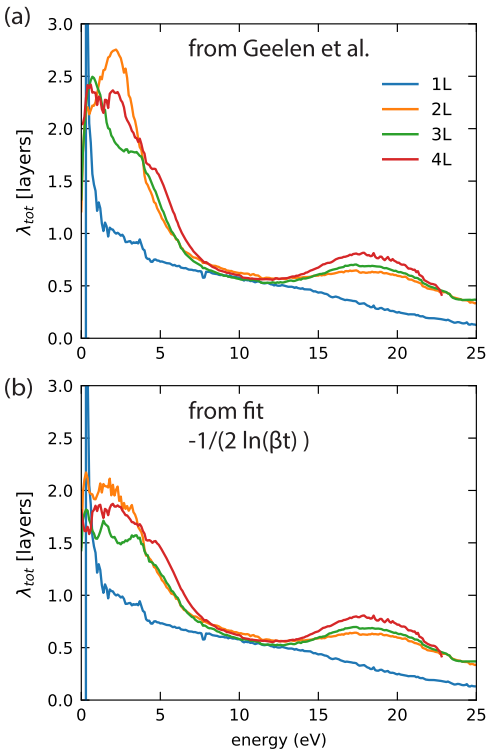

Fig. 5. Total MFP obtained by Geelen et al. [4] (a) compared to the outcome of the fit (b). In the present study the loss factor β and the transmissivity factor t were fitted, yielding the flux transmitted through one layer $(\beta t)^2$. The total MFP in (b) shows less variation at low energy, as the elastic interference peaks are absorbed into the fitted model.

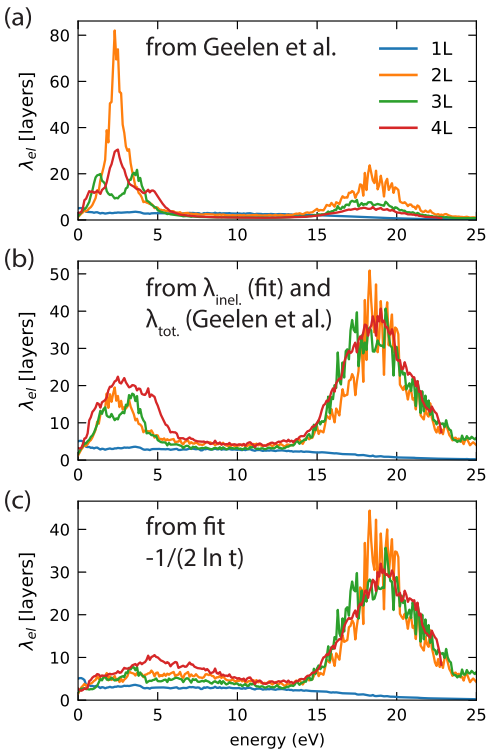

Fig. 6. The energy dependence of the elastic MFP obtained (a) by Geelen et al. [4], (b) by combining the total MFP from Geelen et al. with the inelastic MFP obtained in this study ($\lambda_{\mathrm{el}}^{-1} = \lambda_{\mathrm{tot}}^{-1} - \lambda_{\mathrm{inel}}^{-1}$), and (c) directly from the fitting parameter t.

resonance (3 eV), the other calculations find the highest maximum at the second (18 eV) resonance. This is caused by the rather macroscopic definition used by Geelen et al., compared to the definition from the wave transmissivity t used here. Whichever definition one follows in a semi-classical model, the enhanced elastic MFP is a measure for enhanced transmission.

4. Conclusions

We have applied an improved version of Geelen et al.'s wave-optical model for electron scattering that reproduces both the elastic features linked to interference of the electron wave, and the inelastic features linked to inelastic losses. In the improved model the loss factor β is applied once at every interaction with a discrete graphene layer, thus describing the multiple-scattering zig-zag path travelled. We obtain the energy-dependent inelastic MFP, which over large ranges closely resembles the analysis of Yang et al. but which does converge at energies around 0 eV, 12 eV *and* 25 eV for the different layer counts. Furthermore, the maximum in the inverse inelastic MFP (minimum in β) around 12 eV is ascribed to the neighboring interference minima rather than to the excitation of the $\pi + \sigma$ plasmon, as done by Yang et al.. This is confirmed by the fact that the inelastic MFP at the $\pi + \sigma$ plasmon excitation is the same for the monolayer and the multilayers. We stress again that all models that define a MFP are semi-classical approximations.

While the definition of elastic MFP is debatable, as it strongly depends on the semi-classical approximations made, the elastic MFP clearly increases to multiple layers in the resonances where elastic transmission increases, depending on layer count. Increased transmission goes hand-in-hand with reduced inelastic loss. A full explanation of this correlation must await a more realistic fully quantum mechanical treatment of electron scattering in multilayer graphene, including inelastic effects.

Declaration of Competing Interest

The authors declare that they have no known competing financial interests or personal relationships that could have appeared to influence the work reported in this paper.

Data availability

Data will be made available on request.

Acknowledgments

We acknowledge Marcel Hesselberth for indispensable technical support and Tobias A. de Jong for valuable discussions and code review.

Funding

This research was supported by the Dutch Research Council (PN, NWO Vrije Programma TNW18.071).

Supplementary materials

Supplementary material associated with this article can be found, in the online version, at doi:10.1016/j.ultramic.2023.113800.

References

[1] S. Tanuma, T. Shiratori, T. Kimura, K. Goto, S. Ichimura, C.J. Powell, Experimental determination of electron inelastic mean free paths in 13 elemental solids in the 50 to 5000 eV energy range by elastic-peak electron spectroscopy, Surf. Interface Anal. 37 (2005) 833–845, https://doi.org/10.1002/sia.2102.

[2] M.P. Seah, W.A. Dench, Quantitative electron spectroscopy of surfaces: a standard data base for electron inelastic mean free paths in solids, Surf. Interface Anal. 1 (1979) 2–11, https://doi.org/10.1002/sia.740010103.
[3] B. Da, J. Liu, M. Yamamoto, Y. Ueda, K. Watanabe, N.T. Cuong, S. Li, K. Tsukagoshi, H. Yoshikawa, H. Iwai, S. Tanuma, H. Guo, Z. Gao, X. Sun, Z. Ding, Virtual substrate method for nanomaterials characterization, Nat. Commun. 8 (2017) 15629, https://doi.org/10.1038/ncomms15629.
[4] D. Geelen, J. Jobst, E.E. Krasovskii, S.J. van der Molen, R.M. Tromp, Nonuniversal transverse electron mean free path through few-layer graphene, Phys. Rev. Lett. 123 (2019), 086802, https://doi.org/10.1103/PhysRevLett.123.086802.
[5] H.T. Nguyen-Truong, B. Da, L. Yang, Low-energy electron inelastic mean free path for monolayer graphene Low-energy electron inelastic mean free path for monolayer graphene, 033103 (2020). https://doi.org/10.1063/5.0016284.
[6] Z. Dai, Z. Gao, S.S. Pershoguba, N. Tiwale, A. Subramanian, Q. Zhang, C. Eads, S. A. Tenney, R.M. Osgood, C.Y. Nam, J. Zang, A.T.C. Johnson, J.T. Sadowski, Quantum-well bound states in graphene heterostructure interfaces, Phys. Rev. Lett. 127 (2021) 86805, https://doi.org/10.1103/PhysRevLett.127.086805.
[7] L.H. Yang, B. Da, H. Yoshikawa, S. Tanuma, J. Hu, J.W. Liu, D.M. Tang, Z.J. Ding, Low-energy electron inelastic mean free path and elastic mean free path of graphene, Appl. Phys. Lett. 118 (2021), 053104, https://doi.org/10.1063/5.0029133.
[8] T. Eberlein, U. Bangert, R.R. Nair, R. Jones, M. Gass, A.L. Bleloch, K.S. Novoselov, A. Geim, P.R. Briddon, Plasmon spectroscopy of free-standing graphene films, Phys. Rev. B - Condens. Matter Mater. Phys. 77 (2008) 1–4, https://doi.org/10.1103/PhysRevB.77.233406.
[9] N. Barrett, E.E. Krasovskii, J.M. Themlin, V.N. Strocov, Elastic scattering effects in the electron mean free path in a graphite overlayer studied by photoelectron spectroscopy and LEED, Phys. Rev. B - Condens. Matter Mater. Phys. 71 (2005) 1–9, https://doi.org/10.1103/PhysRevB.71.035427.
[10] D.J. Griffiths, Time-independent schrödinger equation. Introduction to Quantum Mechanics ISBN 0131911759, 2nd ed., 2004.
[11] B. Stec, C. Jędrzejek, Resonance scattering by a double square-well potential, Eur. J. Phys. 11 (1990) 75–81, https://doi.org/10.1088/0143-0807/11/2/002.
[12] N. Ismail, C.C. Kores, D. Geskus, M. Pollnau, Fabry-Pérot resonator: spectral line shapes, generic and related airy distributions, linewidths, finesses, and performance at low or frequency-dependent reflectivity, Opt. Express. 24 (2016) 16366, https://doi.org/10.1364/OE.24.016366.
[13] H. Hibino, H. Kageshima, F. Maeda, M. Nagase, Y. Kobayashi, Y. Kobayashi, H. Yamaguchi, Thickness determination of graphene layers formed on SiC using low-energy electron microscopy, E-J. Surf. Sci. Nanotechnol. 6 (2008) 107–110, https://doi.org/10.1380/ejssnt.2008.107.
[14] P. Virtanen, R. Gommers, T.E. Oliphant, M. Haberland, T. Reddy, D. Cournapeau, E. Burovski, P. Peterson, W. Weckesser, J. Bright, S.J. van der Walt, M. Brett, J. Wilson, K.J. Millman, N. Mayorov, A.R.J. Nelson, E. Jones, R. Kern, E. Larson, C. J. Carey, İ. Polat, Y. Feng, E.W. Moore, J. VanderPlas, D. Laxalde, J. Perktold, R. Cimrman, I. Henriksen, E.A. Quintero, C.R. Harris, A.M. Archibald, A.H. Ribeiro, F. Pedregosa, P. van Mulbregt, A. Vijaykumar, A. Pietro Bardelli, A. Rothberg, A. Hilboll, A. Kloeckner, A. Scopatz, A. Lee, A. Rokem, C.N. Woods, C. Fulton, C. Masson, C. Häggström, C. Fitzgerald, D.A. Nicholson, D.R. Hagen, D. V. Pasechnik, E. Olivetti, E. Martin, E. Wieser, F. Silva, F. Lenders, F. Wilhelm, G. Young, G.A. Price, G.L. Ingold, G.E. Allen, G.R. Lee, H. Audren, I. Probst, J. P. Dietrich, J. Silterra, J.T. Webber, J. Slavič, J. Nothman, J. Buchner, SciPy 1.0: fundamental algorithms for scientific computing in Python, Nat. Methods 17 (2020) 261–272, https://doi.org/10.1038/s41592-019-0686-2.
[15] V.U. Nazarov, Electronic excitations in quasi-2D crystals: what theoretical quantities are relevant to experiment? New J. Phys. 17 (2015), 073018 https://doi.org/10.1088/1367-2630/17/7/073018.
[16] W.S.M. Werner, A. Bellissimo, R. Leber, A. Ashraf, S. Segui, Reflection electron energy loss spectrum of single layer graphene measured on a graphite substrate, Surf. Sci. 635 (2015) L1–L3, https://doi.org/10.1016/j.susc.2014.12.016.
[17] I. Konvalina, B. Daniel, M. Zouhar, A. Paták, I. Müllerová, L. Frank, J. Piňos, L. Průcha, T. Radlička, W.S.M. Werner, E.M. Mikmeková, Low-energy electron inelastic mean free path of graphene measured by a time-of-flight spectrometer, Nanomaterials 11 (2021) 2435, https://doi.org/10.3390/nano11092435.
[18] J. Lu, K.P. Loh, H. Huang, W. Chen, A.T.S. Wee, Plasmon dispersion on epitaxial graphene studied using high-resolution electron energy-loss spectroscopy, Phys. Rev. B - Condens. Matter Mater. Phys. 80 (2009) 2–5, https://doi.org/10.1103/PhysRevB.80.113410.
[19] S.C. Liou, C.S. Shie, C.H. Chen, R. Breitwieser, W.W. Pai, G.Y. Guo, M.W. Chu, Π-plasmon dispersion in free-standing graphene by momentum-resolved electron energy-loss spectroscopy, Phys. Rev. B - Condens. Matter Mater. Phys. 91 (2015) 1–7, https://doi.org/10.1103/PhysRevB.91.045418.